applied sciences

MDPI

Article

Mechanical Study of a Single-Cylinder High-Pressure Steam Engine with a Corliss Valve Gear Using Finite Element Method

José Ignacio Rojas-Sola [1,*] and Santiago Sánchez-García [2]

[1] Department of Engineering Graphics, Design and Projects, University of Jaen, 23071 Jaen, Spain
[2] Higher Polytechnic School, University of Jaen, 23071 Jaen, Spain
* Correspondence: jirojas@ujaen.es; Tel.: +34-953-212452

Abstract: This investigation analyzes the design integrity from a mechanical engineering perspective of a single-cylinder high-pressure steam engine with a Corliss valve gear designed by Arnold Throp. This concerns a double-acting steam engine that incorporates a steam distribution system using a Corliss valve gear, whose blueprints were published in the Model Engineer magazine in 1982. This is a complex historical invention given the high number of components (120) that constitute it, and for which no information exists regarding its operating conditions. Once the 3D CAD model of the same was obtained, and given that no physical model exists to subject to testing, a linear static analysis was performed at two critical positions (top dead center and bottom dead center), determining the maximum gauge pressure at the steam inlet (working pressure), such that the minimum safety factor is within an optimal range with values between 2 and 4. Said linear static analysis was performed using the stress analysis module of Autodesk Inventor Professional 2024, applying the finite element method. The results obtained confirm that the optimal range of working pressures is between 4.1 and 7.8 MPa.

Keywords: steam engine; Corliss valve gear; engineering graphics; computer-aided engineering; mechanical engineering; finite-element analysis; technical historical heritage

Academic Editor: Wei Li

Received: 28 March 2025
Revised: 21 April 2025
Accepted: 24 April 2025
Published: 25 April 2025

Citation: Rojas-Sola, J.I.; Sánchez-García, S. Mechanical Study of a Single-Cylinder High-Pressure Steam Engine with a Corliss Valve Gear Using Finite Element Method. *Appl. Sci.* **2025**, *15*, 4782. https://doi.org/10.3390/app15094782

1. Introduction

Steam engines, historically significant and extensively studied, have been integrated into diverse modes of transportation, including railways, ships, and other forms of locomotion [1,2]. Their fundamental operating principle relies on harnessing the thermal energy of steam, specifically the thermal gradient between the inlet and outlet temperatures, to convert it into mechanical energy that performs mechanical work. This process has been the subject of numerous investigations across various disciplines, such as thermodynamics [3] and fluid mechanics [4,5], among others.

The present study aligns with the research area concerning technical historical heritage, with a particular focus on examining various historical inventions related to the technological advancements experienced by steam engines. The significance of such investigations is evidenced by the numerous conferences dedicated to the Science and History of Machines and Mechanisms [6–8], which reflect the current state of the History of Science and Technology.

Specifically, this study focuses on the investigation of a historical invention by Arnold Throp, published in the magazine Model Engineer in 1982 [9,10], the plans of which were reproduced by Julius de Waal in 2018 [11]. This historical invention has been recently analyzed by the authors from a design perspective [12], detailing the Corliss valve gear

employed in this engine, as there is a lack of available information regarding the invention's operation (steam pressures during admission) and design.

Therefore, this is research in the field of industrial archeology [13], and although this investigation does not indicate new advances in the field of mechanical engineering, it is a noteworthy scientific contribution in the area of technical historical heritage, which studies relevant inventions that represented a milestone in technological development in the 20th century.

George Henry Corliss was an American engineer who made significant contributions to the efficiency of steam engines through the design of valves and governors. The Corliss valve gear, patented in 1849, improved the efficiency of fuel engines by 30% compared to hydraulic engines, leading to its widespread adoption in stationary engines [14] that transmitted mechanical energy to dynamos for electricity generation. Furthermore, these engines have been studied from various perspectives, including their influence on economics [15,16], exhibitions [17,18], and urban development [19].

Given the absence of any information pertaining to the mechanical engineering aspects of the invention worldwide, the research conducted is entirely novel, original, and significant from a scientific standpoint, filling an existing gap in the study of technological development of its time.

Furthermore, no physical model of the aforementioned invention exists. Therefore, the mechanical study to be performed must rely on the faithful 3D CAD model obtained in the previous research [12] carried out by the authors.

Consequently, the ultimate goal of this research is to conduct a design integrity study of the invention, performing a static linear analysis [20] using the finite element method (FEM) [21,22] to characterize its mechanical behavior. This will determine the range of steam pressures at admission (working pressures) that the machine should have to obtain a minimum safety factor value between 2 and 4, established as the optimal design range in current understanding of materials' strength. This approach will ensure that the steam engine operates under safe conditions.

To this end, the different sections of this article are structured as follows: Section 2 presents the materials and methodology followed in the study. Section 3 presents the main results. Section 4 discusses potential model optimizations. Finally, Section 5 presents the main conclusions and future works of this research.

2. Materials and Methods

Given the absence of a physical prototype of the invention upon which mechanical testing could be conducted, the foundational element of the current research was a reliable 3D CAD model of the historical invention. This model was developed based on graphical information reproduced by Julius de Waal [11] from the invention's plans published in the Model Engineer magazine in 1982 [9,10], with simulations performed using Autodesk™ Inventor Professional™ 2024 software [23]. Specifically, a linear static analysis was executed on the 3D CAD model using FEM, facilitated by the stress analysis module integrated within the aforementioned software.

Furthermore, as the operational conditions of the invention are entirely unknown, an iterative process was necessary to determine the steam pressure at the admission (working pressure) point to enable the execution of various simulations and calculations. This iterative process was executed by modifying the working pressure at the piston's impingement surface. The value of this pressure was based on the safety factor derived from each preceding analysis, as this factor was required to fall within the optimal design range of 2 to 4 inclusive. Consequently, the intake pressure result is deemed satisfactory if it resides within this defined range. Therefore, the maximum and minimum pressure

values analyzed in this article are a direct outcome of this iterative process. Consequently, once working pressure was established, a modal analysis and a linear static analysis were performed. These analyses examined the von Mises stresses, displacements, and the safety factor, which characterize the mechanical behavior of the ensemble. This approach allowed for the verification of the invention's design integrity under anticipated real-world operating conditions.

2.1. Operation of the Machine

Although the design and operation of the invention have been studied in detail in a previous publication [12], a brief description of the ensemble and its operation is provided below to enhance the reader understanding. Figures 1 and 2 depict two conical perspectives of the historical invention, highlighting the most notable elements.

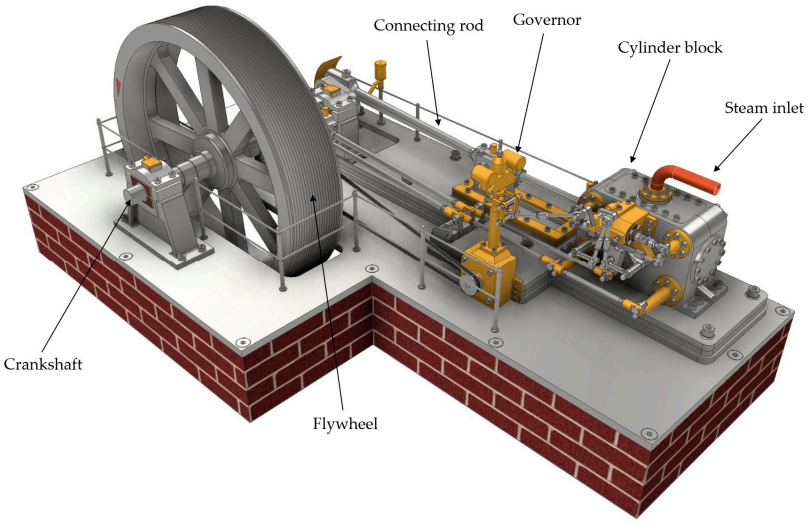

Figure 1. Front conical perspective of the ensemble.

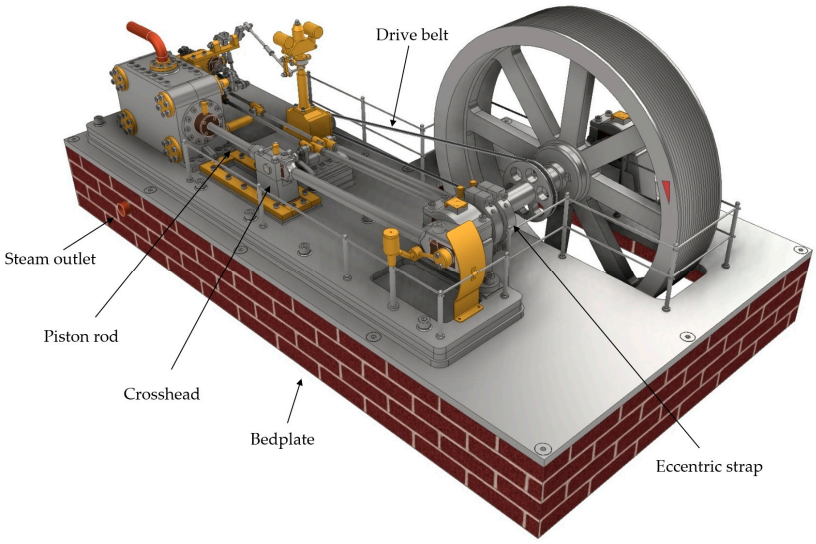

Figure 2. Rear conical perspective of the ensemble.

This high-pressure steam engine consists of a single horizontal double-acting cylinder, meaning that the working fluid enters and exits on both sides of the piston, enabling the simultaneous execution of two thermodynamic cycles, albeit out of phase. That is, when steam is admitted on one side of the cylinder, it is expelled from the other chamber. This linear motion of the piston rod is transformed into an angular motion at the crankshaft by

means of the crosshead and the connecting rod, causing the flywheel to rotate integrally (Figure 3).

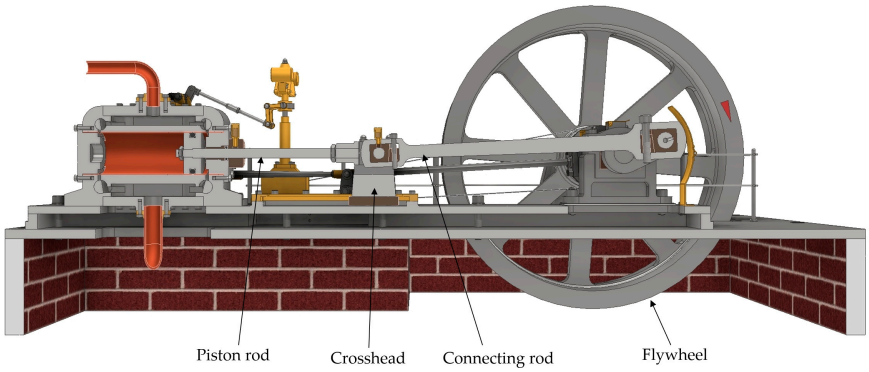

Figure 3. Cross-section of the ensemble.

Furthermore, the crankshaft houses two eccentrics, offset 20° from each other and enclosed by two eccentric straps, to synchronize the opening and closing of the admission and exhaust valves (Figure 4). The speed of the movement is transmitted to the exhaust and inlet valves, with the eccentric closest to the flywheel controlling the exhaust, and the adjacent eccentric controlling the admission (Figure 5).

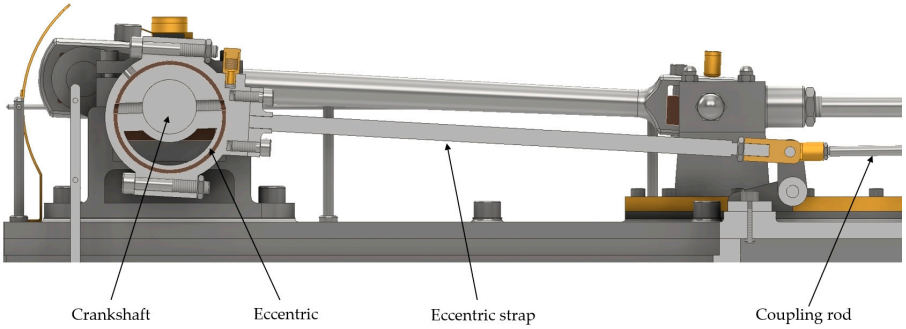

Figure 4. Cross-section showing the eccentric ensemble.

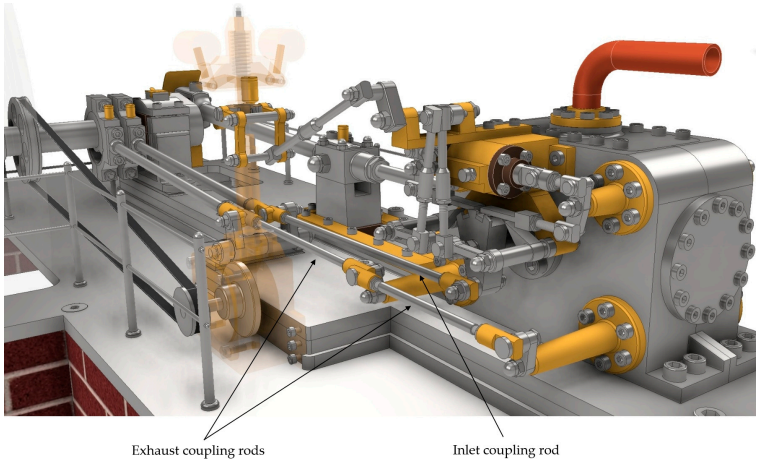

Figure 5. Valve actuation system.

The Corliss valve gear, in addition to controlling the position of the valves to admit and exhaust steam through the connection with the crankshaft by means of inlet and exhaust coupling rods (Figure 5), is also self-regulating due to the presence of the governor. The governor's function is to regulate speed through a linkage system that controls the position

of the cams, being connected to the crankshaft by means of the drive belt and the governor shaft (Figure 6). Thus, if the invention experiences an increase in speed, due to centrifugal force, the flyweights will open, causing the dashpot spring housed within to contract, and consequently, the glut collar to rise. This causes the cam levers to reduce their vertical inclination and brake the trip blades, which are directly connected to the admission valves. The opposite occurs when it experiences a decrease in speed, causing the admission to accelerate.

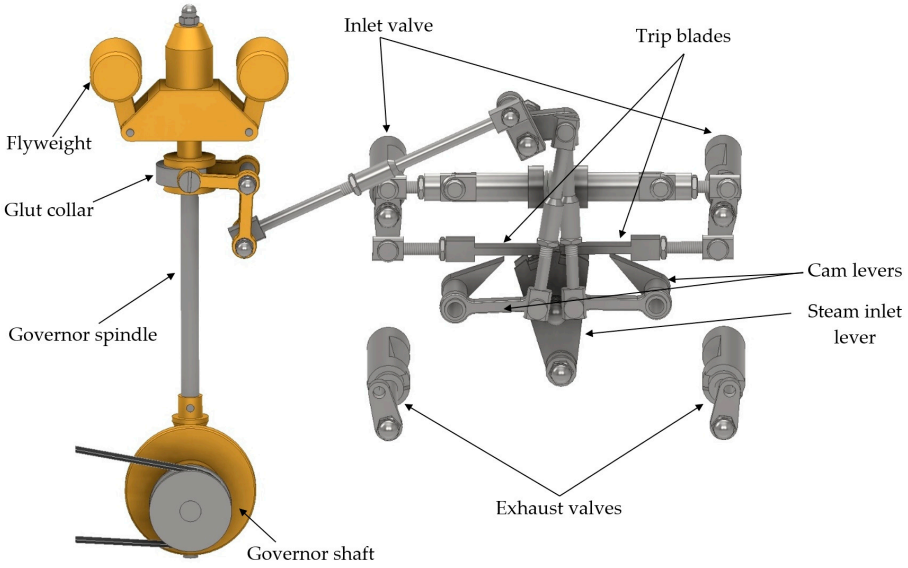

Figure 6. Corliss valve gear.

2.2. Mechanical Engineering Analysis

This section outlines the methodology employed to conduct the linear static analysis using FEM, as well as the working hypotheses established at the various stages. Figure 7 shows a flowchart with those stages:

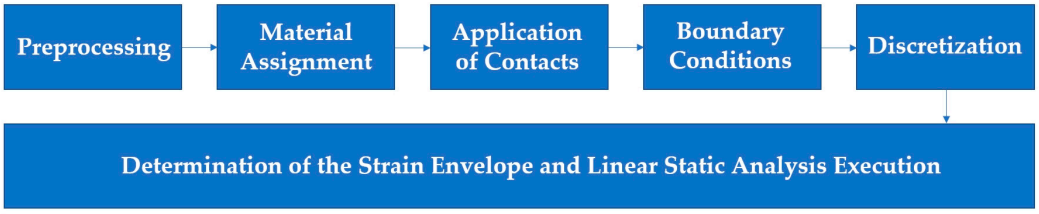

Figure 7. Flowchart of the stages to conduct the linear static analysis using FEM.

2.2.1. Preprocessing

The linear static analysis can be performed considering the complete 3D CAD model that incorporates all the components of the steam engine. However, to reduce simulation time and computational cost, the decision was made to eliminate those elements that do not influence the simulation in relation to the two critical positions identified.

For this reason, all threaded connections such as bolts and nuts, among others, have been removed and replaced by 'Bonded' type contacts between elements. Decorative fillets and chamfers have also been removed, except for those of the cylinder block and the engine bedplate, as they are located in an area of the steam engine subject to stresses. Similarly, handrails and oilers with decorative purposes have also been removed, maintaining only the banjo oiler at the connecting rod and crankshaft joint, attached to the crankshaft, as it is located in a position susceptible to stresses and displacements. Furthermore, the flywheel has been simplified, eliminating the toothed surface and fillets in its structure.

Finally, since this is a linear static analysis, and not a dynamic analysis, the drive belt, governor, and linkage system that self-regulate speed by modifying the inclination of the cams, as mentioned previously, have been removed, as there is no information about the rotational speed and, therefore, they have not been considered in the linear static analysis.

Figures 8 and 9 show the simplified ensemble of the historical invention with which the linear static analysis will be performed.

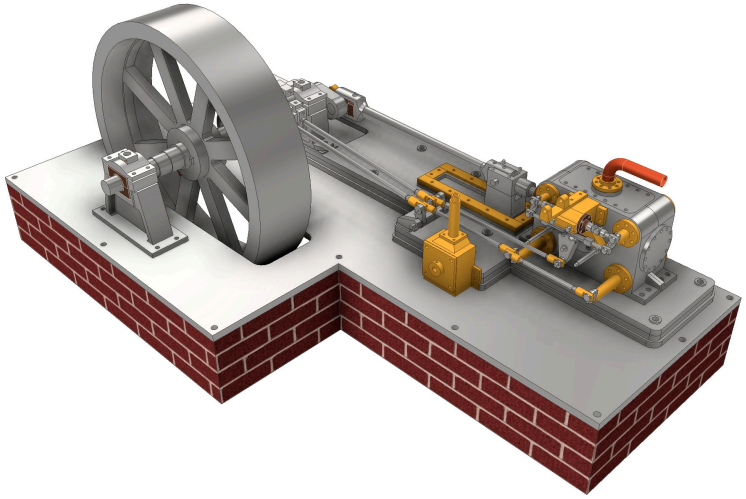

Figure 8. Front conical perspective of the simplified ensemble.

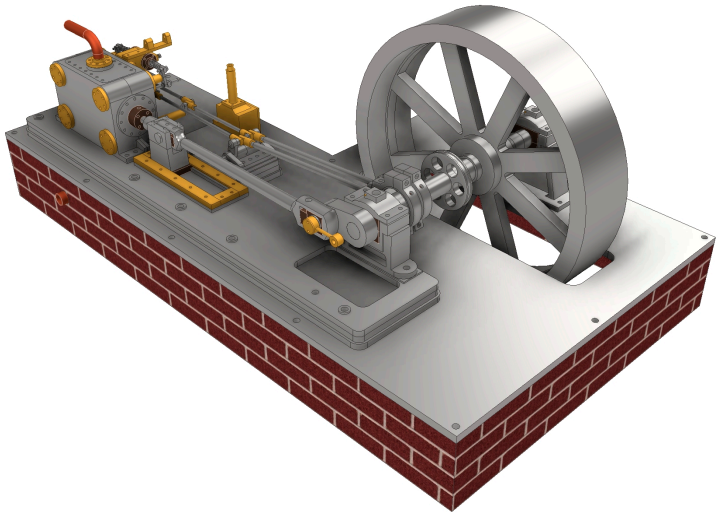

Figure 9. Rear conical perspective of the simplified ensemble.

2.2.2. Material Assignment

In this stage, materials are assigned to each component of the 3D CAD model to attribute the corresponding mechanical properties, which is crucial as it defines its mechanical behavior. In the case of this research, the materials were assigned from the material library offered by Autodesk Inventor Professional 2024, except for the brick, whose properties do not appear in the database and were added by making a simplification. Furthermore, brick does not have a linear behavior, as it is fragile and anisotropic, and also considering that the bedplate is formed by bricks adhered to each other with cement, forming a composite material. Therefore, as a simplification, it has been assumed that the bedplate has the homogeneous properties of a pressed clay-brick.

Furthermore, the basic components of the invention, such as the flywheel, crankshaft, connecting rod, and crosshead, have been designed using mild steel. However, stainless

steel is employed for the piston rod and piston head due to their direct contact with steam within the cylinder. Similarly, components in continuous contact with steam, including the intake and exhaust pipes, as well as the cylinder liner, are composed of copper. Finally, other notable basic elements, such as the springs located within the governor and the control unit, have been designed using AISI 1080 steel.

Table 1 indicates the materials and their main mechanical properties used in the linear static analysis.

Table 1. Properties of each material used in the analysis.

Material	Young's Modulus (MPa)	Poisson Coefficient	Density (kg/m^3)	Yield Strength (MPa)
AISI 1080 Steel	195,000	0.300	7850	206.84
Brick	7000	0.210	2150	5.00
Brass	109,600	0.330	8470	103.40
Cast Bronze	109,600	0.340	8870	128.00
Copper	117,500	0.340	8940	46.00
Mild Steel	220,000	0.280	7850	250.00
Rubber	3000	0.490	1250	10.34
Stainless Steel	193,000	0.300	8000	250.00

2.2.3. Application of Contacts

To perform a reliable simulation using FEM, it is necessary to determine the existing contacts between the elements that comprise the ensemble. Autodesk Inventor Professional 2024 allows for the automatic creation of contacts, applying the 'Bonded' contact to all elements, which does not accurately reflect reality. This poses a drawback, necessitating the manual modification of certain components to avoid a time-consuming process due to the large number of contacts. Among the contacts to be selected manually, the most appropriate type can be applied, with the following being particularly noteworthy:

- Bonded contact: Assumes the rigid fixation of contact faces to each other, preventing them from moving or deforming relatively between other components. It is primarily used for threaded connections, welds, or bonded parts.
- Separation contact: Assumes the total or partial separation of contact faces when they slide during the analysis, allowing space between components. This allows components to move when applied forces exceed a certain limit. It is used in modeling where parts are expected to separate, such as in crack opening or component separation itself.
- Sliding contact: Assumes the fixation of contact faces in the perpendicular direction of the face while sliding in a specific direction. It is used in situations where sliding is expected, such as in guides.
- Separation/no-slide contact: Assumes total or partial contact separation without sliding them against each other. It is used when there is high friction or locking under certain conditions, such as in the case of a rubber part on rough surfaces.
- Sliding/shrink fit contact: Provides conditions such as 'separation' with components initially overlapped, and therefore, the initial distance between contact faces is negative. It is used for joints where there is a clearance tolerance.
- Non-sliding/shrink fit contact: Provides separation conditions without sliding with initially overlapped parts. Used in joints where there is an interference fit tolerance.
- Spring contact: Creates equivalent springs between two faces, allowing the definition of total tangential and normal stiffness. It is used to simulate contacts that require controlled compression or expansion forces, such as in elastic elements or suspensions.

Subsequently, several examples of the contact types utilized in the assembly are illustrated. Figure 10 depicts the application of a bonded contact between the bedplate and the crankshaft support, employed to simplify the model by eliminating the representation of screws.

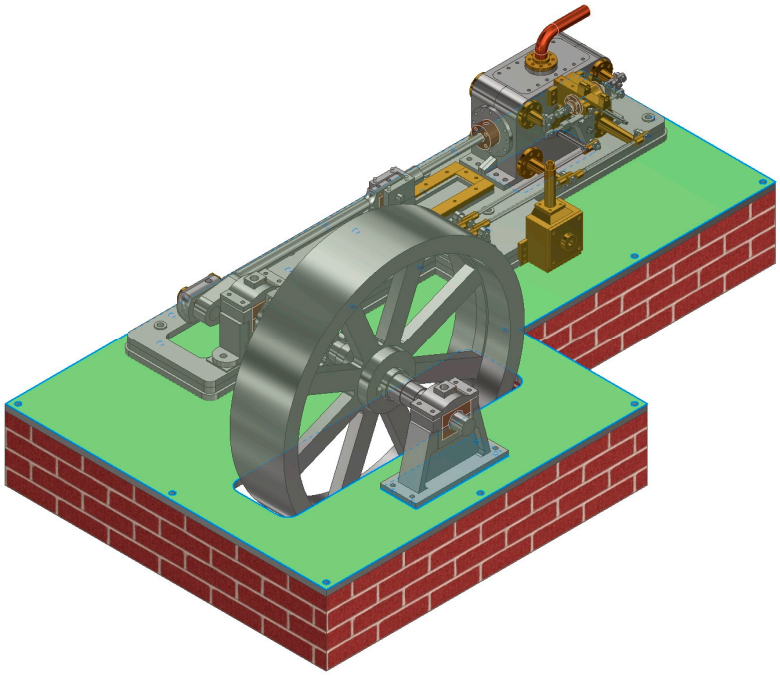

Figure 10. Example of application of bonded contact.

Figure 11 shows the implementation of a sliding contact between the piston rod and the cylinder front cover. Finally, Figure 12 illustrates the application of a spring contact to the spring located within the control unit and the wall of the dashpot housing, with an identical independent application at the opposing end.

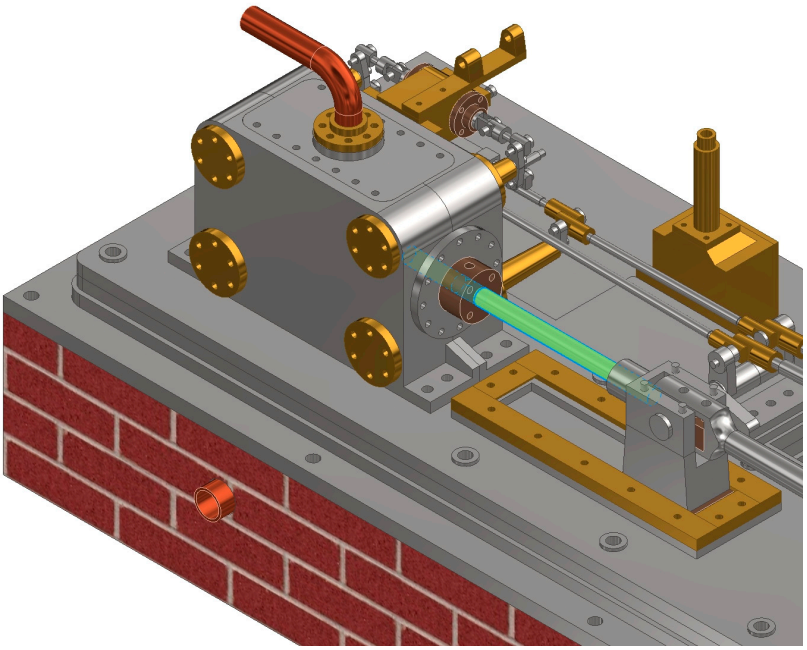

Figure 11. Example of application of sliding contact.

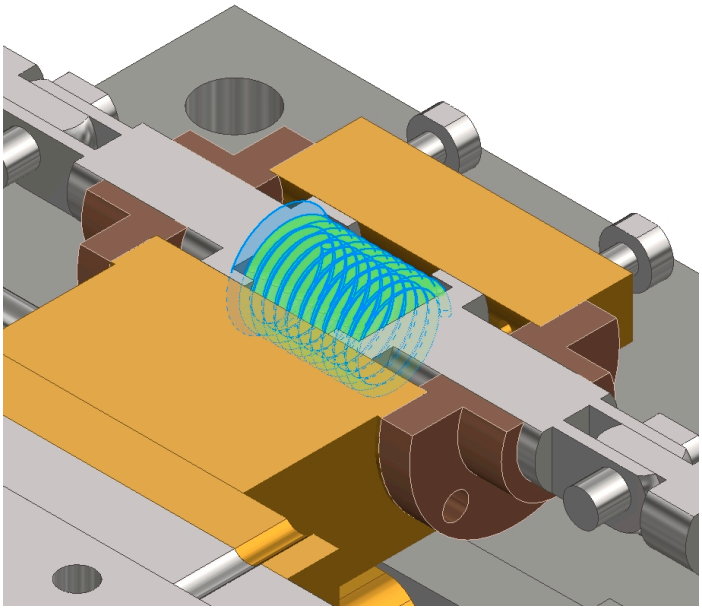

Figure 12. Example of application of spring contact.

The majority of applied contacts are of the 'bonded' and 'sliding contact' types, specifically for the contacts of the valves and piston within the cylinder block, as well as for the crosshead. Furthermore, each contact type can be symmetric, where mesh nodes cannot penetrate adjacent mesh nodes, or asymmetric, where such penetration is allowed.

In the case of the dashpot spring housed within the dashpot control unit, a 'spring contact' type was employed, considering the material it is composed of (AISI 1080 steel with a shear modulus (G) of 75 GPa), its geometry (with a wire diameter (d) of 1 mm and a mean spring diameter (D) of 5.5 mm), and its configuration of 10 (N) turns, resulting in an equivalent normal stiffness (k) of 5.635 N/mm.

$$k = \frac{Gd^4}{8D^3N} \tag{1}$$

2.2.4. Boundary Conditions

Boundary conditions were applied to the bedplate and the flywheel (Figure 13) by fixing or constraining the six degrees of freedom, with the aim of performing an analysis that simulates the connection of the bedplate to another solid on the lower surface of this component. Regarding the flywheel, a fixed constraint was applied to the outer surface to simulate one of the critical positions, specifically when the flywheel is locked, which occurs when the invention is stopped and its operation is to be initiated. This constraint of the six degrees of freedom causes motor torque to be transmitted to the cylinder block.

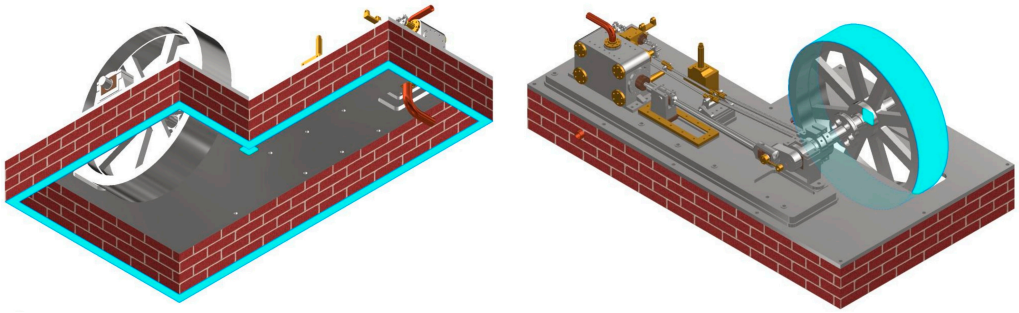

Figure 13. Restriction of the six degrees of freedom of the bedplate and the flywheel.

2.2.5. Discretization

The next stage in the analysis process is the discretization of the model. Numerous publications detail the discretization stage as a fundamental part of the finite element method [24–26]. Based on these publications, some of its fundamentals are explained below for better reader comprehension.

This stage consists of dividing the model into multiple elements bounded by nodes, forming a mesh. This nodal division is crucial for simplifying calculations, as the analysis variables will be computed at these points. However, the results provided by the software are obtained through the interpolation of each element's nodes, yielding a displacement value per element.

This significantly affects the quality of the results. If the analysis is performed with a very large element size, the result gradients will not be accurately visible, potentially omitting relevant information. Conversely, a small element size results in a greater number of nodes, allowing for more precise value determination. Therefore, a balance between computational cost and result quality must be achieved through element size optimization.

The elements constituting the mesh can be of various types depending on the model's geometry to obtain better results. For three-dimensional elements, these can be tetrahedra, prisms, or hexahedra, differentiated by the number of nodes, which results in distinct shape functions affecting displacement interpolation. These polynomial shape functions ensure displacement continuity within the discretized domain. Furthermore, it is worth mentioning that the ideal element geometry, regardless of type, should have proportional sides. An element with a long side compared to a short side will have poor quality. This is measurable using the Jacobian matrix, which defines the element's shape functions.

Additionally, the differential equations governing the system are discretized, obtaining an algebraic system of equations for each element, such that the global stiffness matrix can be determined by assembling each local stiffness matrix when resolved for an element, correlating nodal displacements with nodal forces.

The equilibrium equations for a continuous system are formulated as partial differential equations:

$$\nabla\sigma + f = 0 \tag{2}$$

where external applied forces are given by the vector f and the internal stress tensor is σ.

Thus, once the boundary conditions, loads, and global stiffness matrix are applied, the system of linear equations can be solved, obtaining as a result the vector of nodal displacements, the system being as follows:

$$f = Ku \tag{3}$$

where the unknown nodal displacements (u) result from the nodal forces (f) and the system's stiffness, represented by the global stiffness matrix (K).

Subsequently, the presentation and interpretation of the results proceed through post-processing tools, allowing the display of displacements, deformations, and stresses in the discretized model, thereby determining the most affected areas and ensuring an integrity criterion regarding the design.

In the case of the present research, the element type employed for discretization was the first-order tetrahedron, as it only has nodes at the vertices of the element (Figure 14). Furthermore, the software generates the mesh automatically, with larger element sizes in larger components and smaller element sizes for smaller components or surfaces, to conform to the geometry.

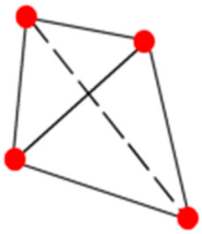

Figure 14. Element used for meshing: first-order tetrahedron.

Furthermore, the configuration for automatic mesh generation involves various factors (with the default values offered by the software, which have been adopted in the present research, in parentheses): average element size as a fraction of the bounding box length (0.1), minimum element size as a fraction of the average size (0.2), element growth gradient factor (1.5), and maximum turn angle (60°).

This configuration provides significant control in mesh generation in contact areas between components. Figure 15 displays the result of the automatic mesh offered by the software, which will serve as the basis for the linear static analysis, except for certain parts where the mesh has been refined and will be discussed later for each critical position studied, imposing the condition that the relative error in von Mises stresses between an iteration j and the previous $j - 1$ must be less than 10%. Thus, the mesh used in the linear static analysis consists of 932,452 nodes and 549,529 elements.

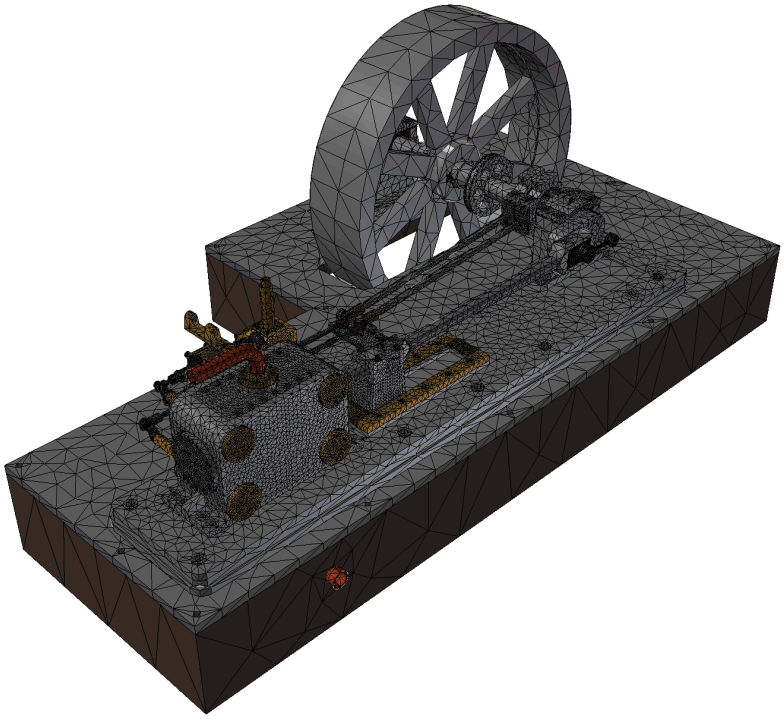

Figure 15. Automatic meshing generated by the software for linear static analysis.

As can be observed in the aforementioned figure, the cylinder block, piston, and crosshead, among others, exhibit a finer mesh, as these are the areas where the highest stresses are expected to occur.

2.2.6. Critical Positions

The determination of critical positions is crucial for understanding the system's behavior under extreme conditions. In a steam engine, two critical positions are typically identified: when the piston, located inside the cylinder block, is at the top dead center

(critical position 1) and at the bottom dead center (critical position 2), with the intake valve closed in both positions. Furthermore, by locking the flywheel during the analysis, it is possible to simulate the invention's behavior during startup and, therefore, the transmission of forces from the piston to the rest of the components.

Figures 16 and 17 show the two critical positions that will be considered in the linear static analysis. In these figures, the positioning of certain components such as the piston rod, crosshead, and connecting rod can be visualized, these being key elements for understanding the critical positions and the design integrity of the invention.

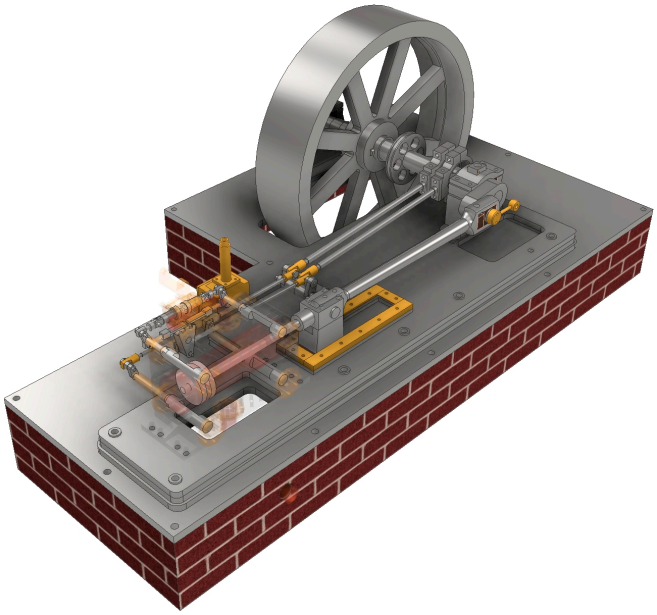

Figure 16. Critical position 1: top dead center.

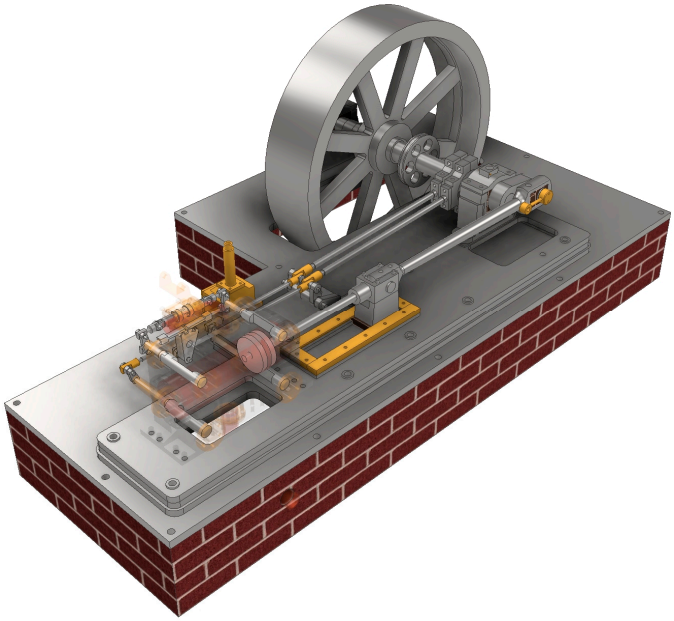

Figure 17. Critical position 2: bottom dead center.

2.2.7. Modal Analysis

Modal analysis is a fundamental tool in mechanical and structural engineering, as its purpose is to elucidate the dynamic behavior of a system composed of multiple components. This type of analysis is employed to determine the natural frequencies (Hz) and vibration

modes of the ensemble, providing essential information about the response to dynamic loads, stability, and potential resonance problems. Each mechanical system has as many natural frequencies as degrees of freedom, potentially reaching a large number of modes. Furthermore, if these natural frequencies are non-zero and distinct from each other, it can be determined that the ensemble not act as a mechanism and, therefore, a linear static analysis can be developed.

2.2.8. Linear Static Analysis

By way of introduction, and based on the numerous existing publications [27–29], which detail the linear static analysis within the finite element method framework, its fundamentals are explained below for a better understanding by the reader.

Linear static analysis can be performed once it is verified that none of the natural frequencies of the different vibration modes is zero. For a better understanding of this stage and the functions integrated into the software, which displays other magnitudes in the post-processing stage, they are explained below, starting from the equation used to obtain the displacement vector (u):

$$u = N\delta^e \tag{4}$$

where for each element, N is the shape function, and δ^e is the nodal displacement vector, providing the 3D relative position and rotation to the reference coordinate axes.

With this, the value of the unit deformations (ε) is obtained:

$$\varepsilon = \partial u = B\delta^e \tag{5}$$

where the relationship between displacements of the element's nodes and the unit deformations at any point within the element are given by the matrix B, which defines the unit deformation field existing inside the element, and δ^e is the nodal displacement vector.

Furthermore, linear static analysis is based on fundamental assumptions such as static equilibrium conditions, linear elasticity, and small deformations. Besides, Hooke's law establishes the following:

$$\sigma = E \cdot \varepsilon \tag{6}$$

where the stress, given by σ, is related to the strain, given by ε, by the Young's modulus or elastic modulus of the material, E.

The assumption of small deformations implies that the original geometry does not change because the changes in the ensemble's geometry are negligible. Furthermore, the static equilibrium conditions require that the sum of forces and moments acting on the system be zero. Additionally, linear static analysis is governed by equilibrium equations where internal forces must be in equilibrium, stress–strain relationships derived from the linear static behavior of materials, and strain compatibility, ensuring they conform to the boundaries and interactions between components.

All of this is defined under differential equations for an axial load P and an internal pressure p acting on the various elements where the load is applied.

Besides, moment equilibrium, axial equilibrium, and transverse equilibrium are represented by Equations (7), (8), and (9), respectively:

$$\frac{dM}{dx} - V = 0 \tag{7}$$

$$\frac{dN}{dx} + q = 0 \tag{8}$$

$$\frac{dV}{dx} + pA = 0 \tag{9}$$

where bending moment is given by M, normal force by N, the distributed force by q, and the shear force by V.

Regarding the stress–strain relationship for axial strain, it is given by the following:

$$\varepsilon_x = \frac{du}{dx} \tag{10}$$

where u represents axial displacement.

The strain for bending deformation is given by the following:

$$\varepsilon_{xx} = \frac{d^2v}{dx^2} \tag{11}$$

where v represents transverse displacement.

On the other hand, to achieve the normal and transverse stresses, these stress–strain relationships are considered using Hooke's law:

$$\sigma_x = E \cdot \varepsilon_x \tag{12}$$

$$\tau_{xy} = G \cdot \gamma_{xy} \tag{13}$$

where the shear modulus is given by G and the shear strain by γ_{xy}.

Thus, considering the applied boundary conditions and loads, the stresses, displacements, and deformations at each point can be determined.

As previously mentioned, for greater accuracy of results, a mesh convergence analysis must be performed, which consists of refining the mesh based on the von Mises stress results until the maximum value does not vary substantially (relative error between iterations less than 10%), thereby optimizing the model to avoid high computational cost.

Furthermore, to conduct a proper analysis, the stress envelope must be established. Thus, gravitational force can be applied by locating it at the center of mass of the ensemble. Since the materials of each component are defined, the software is capable of calculating the mass of each component and, therefore, the location of the ensemble's center of mass.

On the other hand, the complete absence of information regarding the operating conditions of the steam engine in terms of the gauge steam pressure at admission (working pressure) suggests that an iterative process should be followed (varying only the magnitude value of the pressure exerted on the piston head) so that, after performing a linear static analysis, a safety factor value between 2 and 4 is obtained as the optimal design range.

Thus, an initial working pressure of 3.4 MPa was established, typical of some real-world applications such as locomotives. However, the minimum safety factor turned out to be greater than 4, being outside the optimal design range. Therefore, the steam engine components were operating in a very low stress range, considering the material's yield strength, requiring an increase in pressure to be within this optimal design range and ensure proper operation.

After several iterations, it was verified that the most restrictive working pressure is 7.8 MPa when the piston is at the bottom dead center (critical position 2), obtaining a safety factor very close to 2. As for the least restrictive working pressure value, it turned out to be 4.1 MPa, found when the piston is located at the top dead center (critical position 1), with a safety factor close to 4.

Consequently, for the linear static analysis by FEM, the working pressure of 7.8 MPa will be used, analyzing the behavior in both critical positions. Figure 18 shows the steam engine configurations to which the stress envelope will be applied to the piston head and the center of mass.

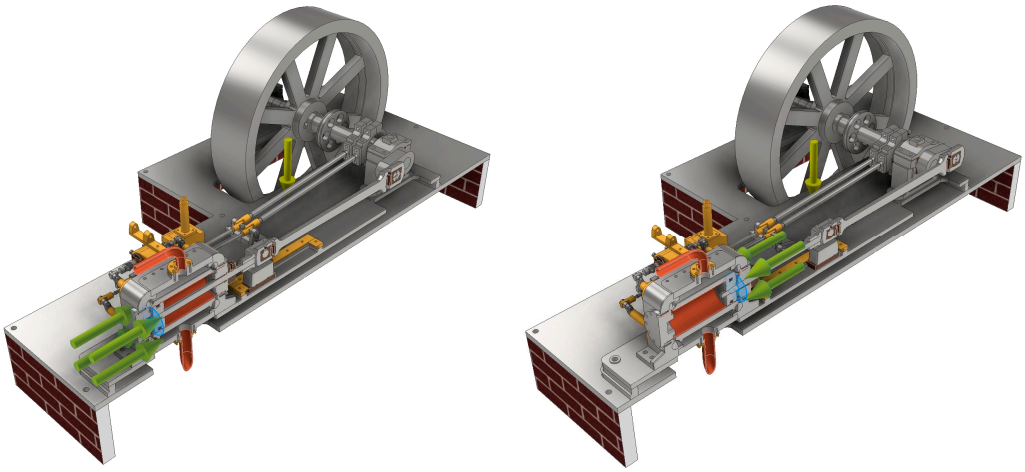

Figure 18. Stress envelope at the two critical positions: top dead center (**left**) and bottom dead center (**right**).

3. Results

3.1. Critical Position 1: Top Dead Center

3.1.1. Modal Analysis

Once the mesh is configured, a modal analysis is performed to determine the natural frequencies of the first ten vibration modes. Figure 19 shows a graph with the analysis results, where the horizontal axis represents the vibration modes, and the vertical axis represents the natural frequency values (Hz), displaying their values for each mode. As can be observed, the obtained results are non-zero and distinct from each other. Therefore, it can be asserted that the system does not behave as a mechanism, and consequently, a linear static analysis can be carried out.

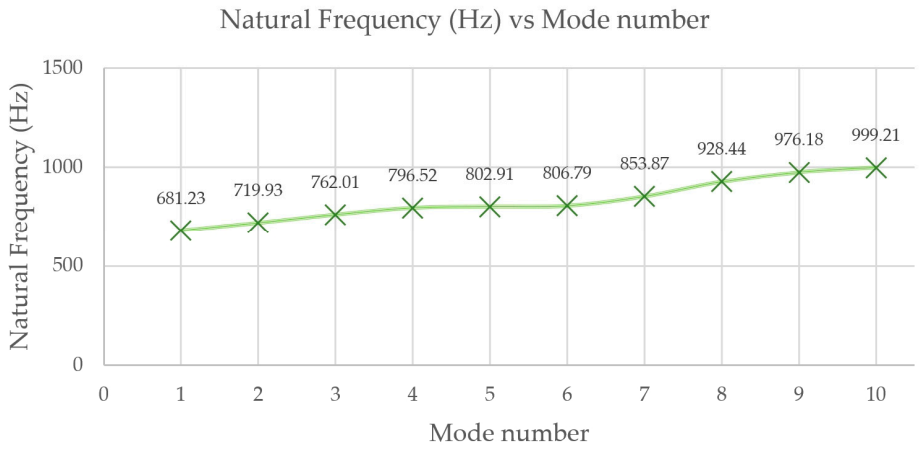

Figure 19. Natural frequencies vs. vibration modes.

As can be observed in the preceding figure, the presented results exhibit an upward trend. Consequently, there is no risk of undesirable behaviors occurring in the invention's operating principle, as this trend inherently mitigates the possibility of resonance.

3.1.2. Linear Static Analysis

As a preliminary step to obtaining results, a mesh convergence analysis must be performed. For critical position 1, the working pressure is 7.8 MPa, as previously mentioned, a result obtained from the iterative process to achieve a safety factor within the optimal design range of 2 to 4, with a value very close to 2 for this position.

Furthermore, in this iterative process, analyses were conducted for gauge pressure values whose safety factors resulted in values below 2, such as in the case of a working pressure of 10 MPa (Figure 20), identifying the most critical component as the piston rod, being the only element that withstands a maximum von Mises stress (Figure 21) (double that withstood by the rest of the components).

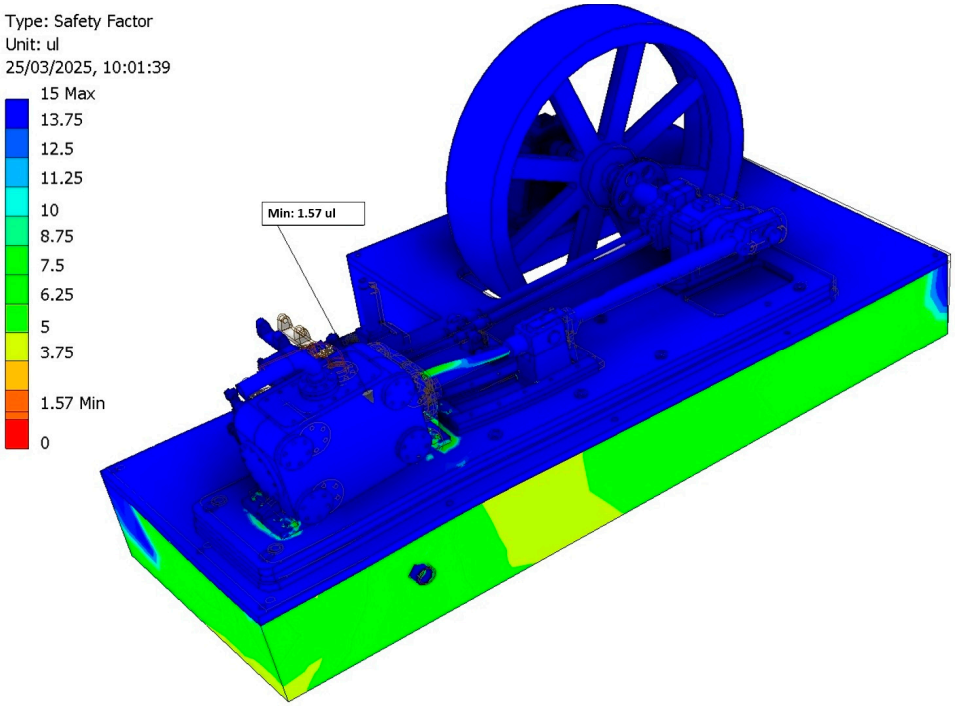

Figure 20. Distribution of the safety factor for a working pressure of 10 MPa.

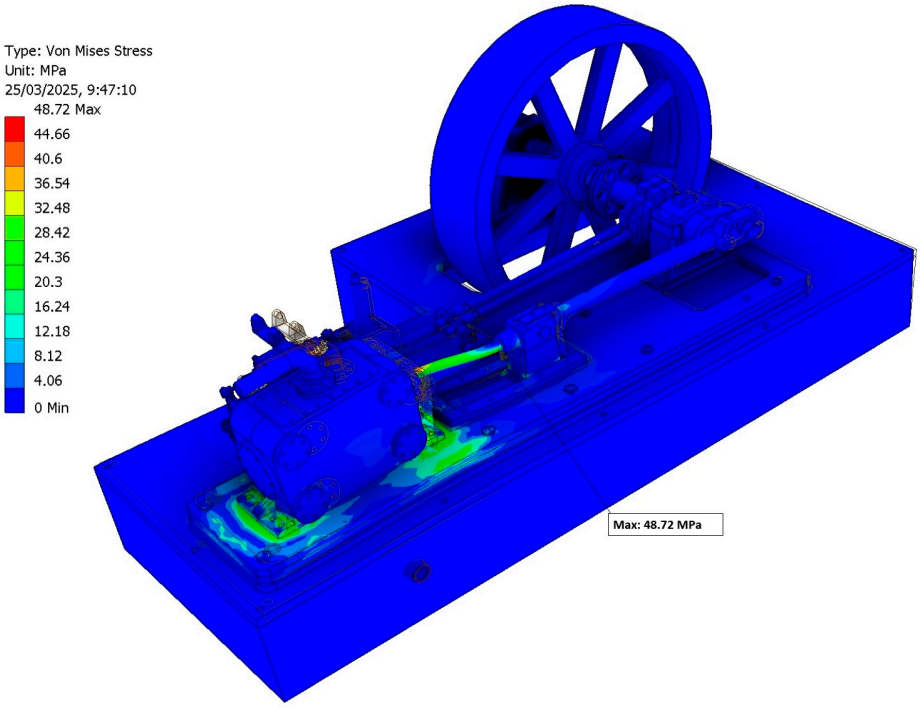

Figure 21. *Cont.*

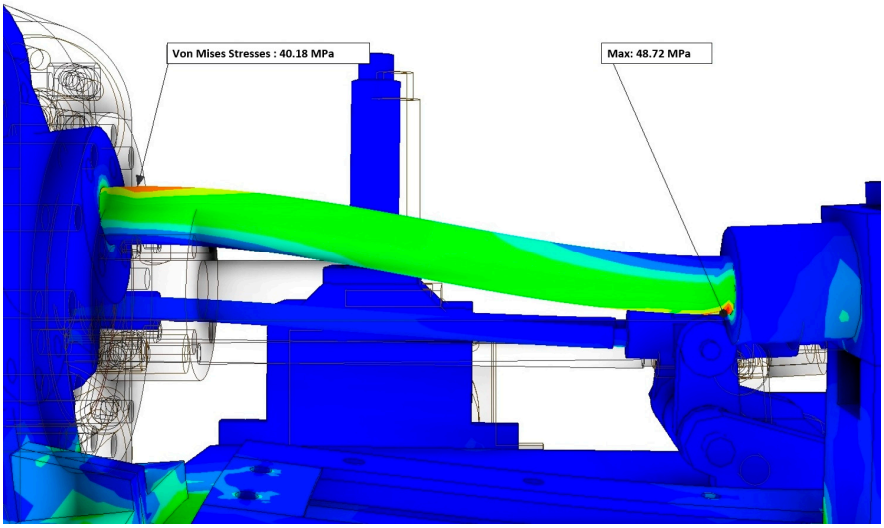

Figure 21. Von Mises stress distribution of the ensemble (**top**) and the piston rod (**bottom**) for a working pressure of 10 MPa.

Therefore, this will be the element to which the mesh convergence analysis is applied under the criterion of a relative error of less than 10% between iterations (Figure 22). Additionally, the element size values, von Mises stress (MPa), and relative error percentage for each iteration are recorded in Table 2.

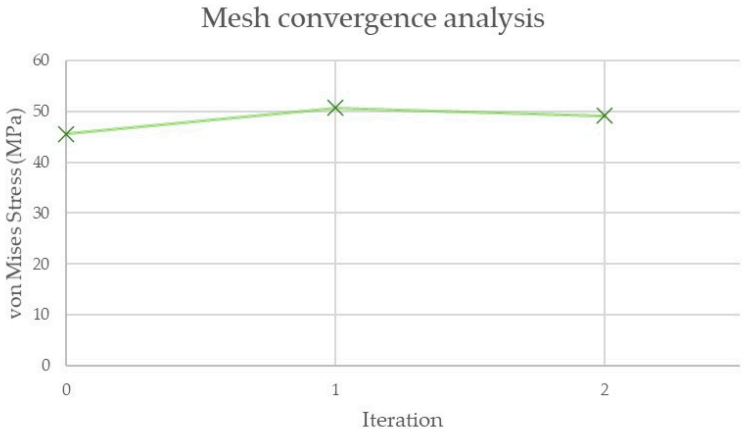

Figure 22. Maximum von Mises stresses obtained at each iteration.

Table 2. Results of mesh convergence analysis.

Element Size (mm)	Von Mises Stress (MPa)	Relative Error (%)	Iteration
5	45.59	Not Available	0
4	50.67	11.14	1
3.8	49.14	3.11	2

Once the mesh convergence analysis was completed, it was concluded that a higher degree of mesh refinement was required, with the element size value for the piston rod being 3.8 mm.

Therefore, the linear static analysis was performed for the previously defined working pressure of 7.8 MPa. Figure 23 shows the von Mises stress distribution of the ensemble, with its maximum value (49.14 MPa) located at the lower part of the piston rod, specifically at the joint with the crosshead (Figure 24).

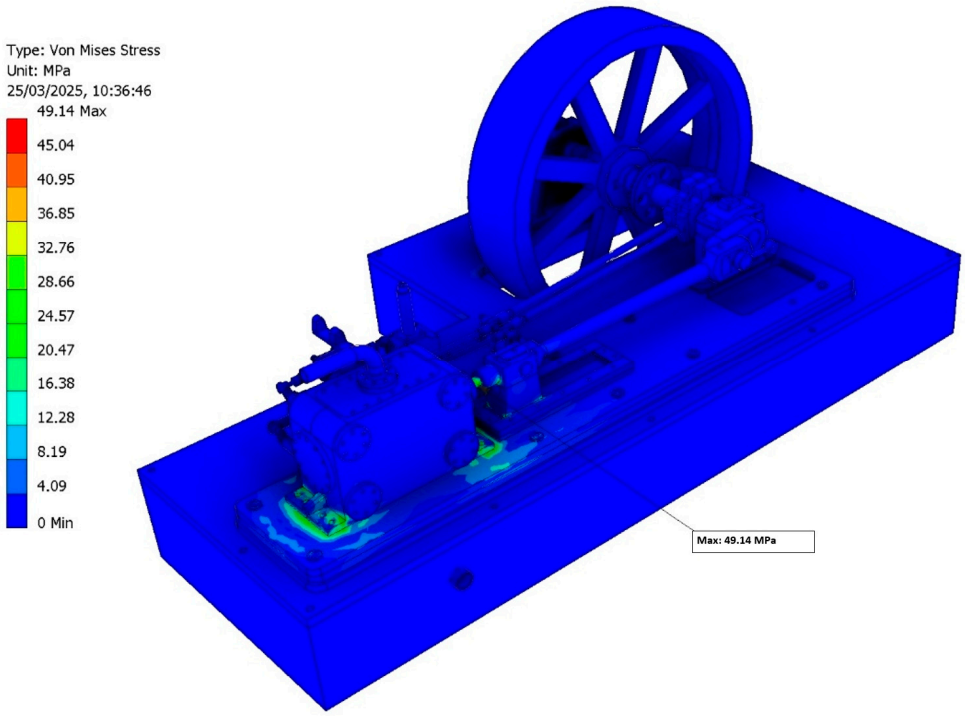

Figure 23. Von Mises stress distribution for a working pressure of 7.8 MPa.

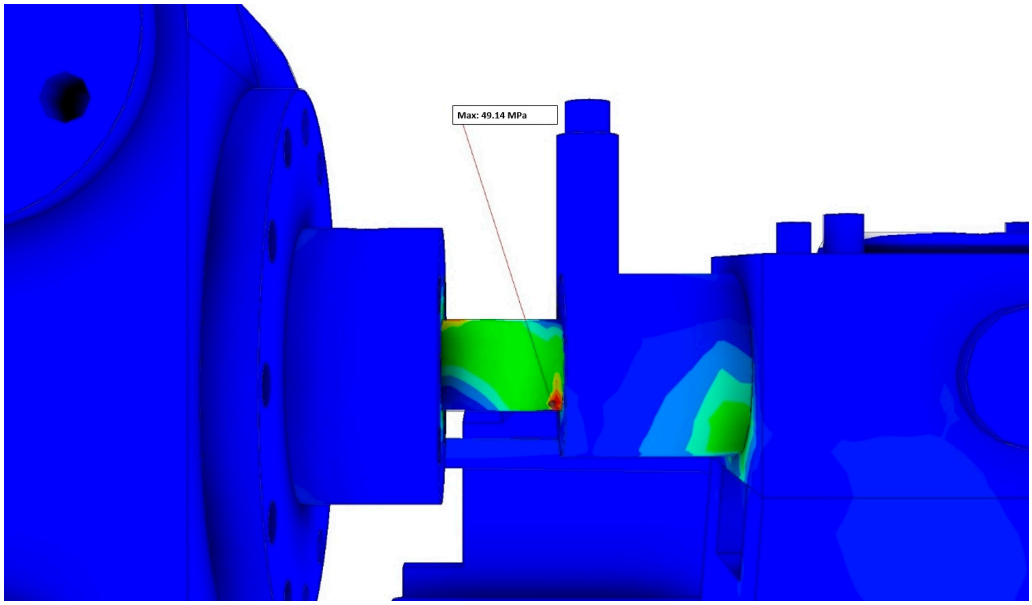

Figure 24. Location of the maximum value of the von Mises stress for a working pressure of 7.8 MPa.

Furthermore, the displacement distribution (Figure 25) was also obtained, shown with a scale factor ($\times 0.5$) for improved visualization. Thus, analyzing the maximum obtained value of 0.04928 mm, located in the inlet steam pipe situated at the top of the cylinder block, it can be considered negligible as it is significantly smaller than the dimensions of the historical invention, considering its operation.

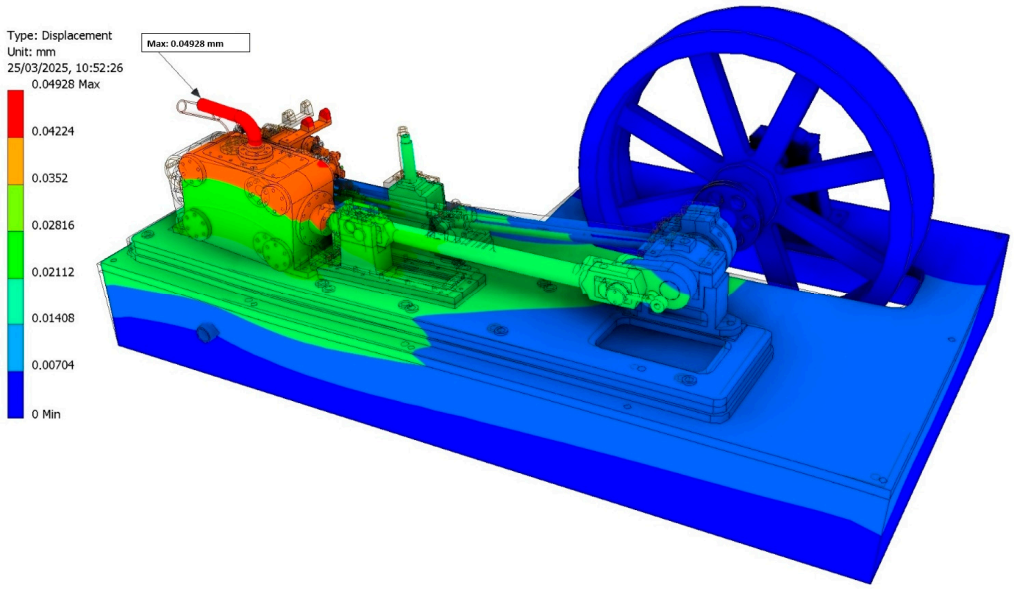

Figure 25. Distribution of displacements and location of the maximum value with a scale factor of ×0.5 for a working pressure of 7.8 MPa.

Finally, the safety factor distribution (Figure 26) and the location of its minimum value (2.09) in the cylinder liner (Figure 27) were also obtained, being within the optimal design range.

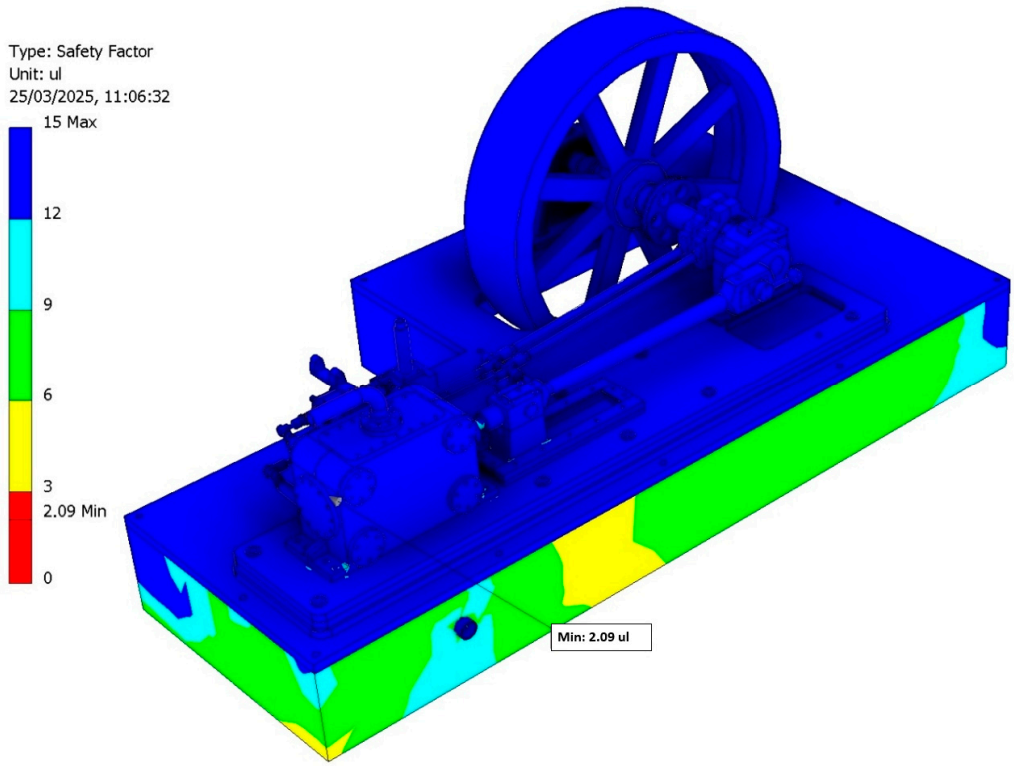

Figure 26. Distribution of the safety factor for a working pressure of 7.8 MPa.

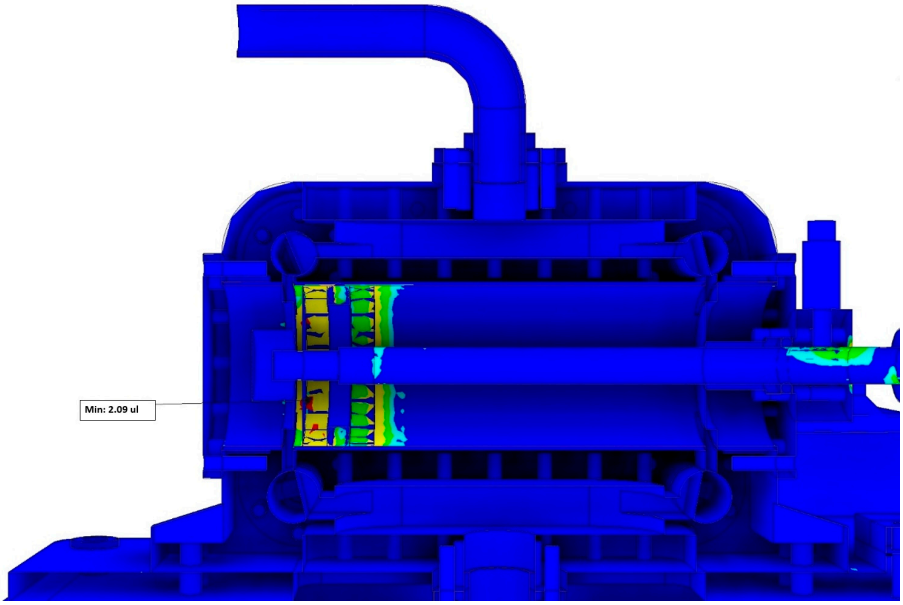

Figure 27. Location of the minimum value of the safety factor for a working pressure of 7.8 MPa.

3.2. Critical Position 2: Bottom Dead Center

3.2.1. Modal Analysis

Analogously, a modal analysis was performed at critical position 2, corresponding to the bottom dead center. Figure 28 shows a graph with the results of this modal analysis, where it can be observed that the obtained results are distinct from each other and none are zero (0 Hz). Therefore, similarly to critical position 1, it is not a mechanism, and consequently, a linear static analysis can be carried out.

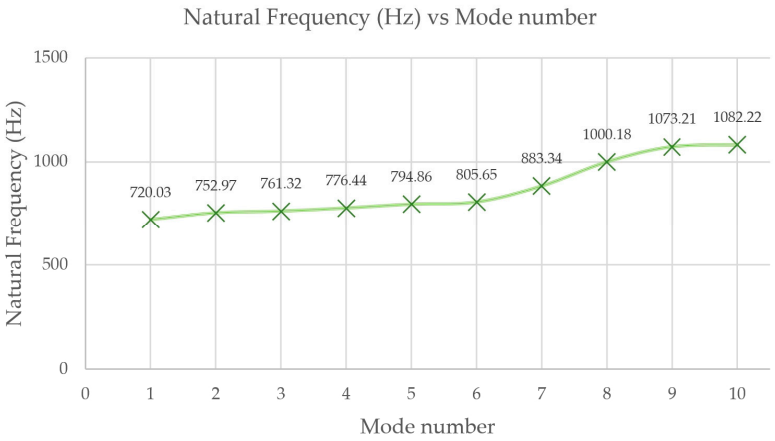

Figure 28. Natural frequencies vs. vibration modes.

Similarly to the previous critical position, the obtained results demonstrate an upward trend. Consequently, there is no risk of undesirable dynamic behaviors occurring in the invention's operating principle, as this trend would impede the onset of resonance.

3.2.2. Linear Static Analysis

Conducting an analysis similar to that performed for critical position 1, a working pressure of 7.8 MPa has been established. Furthermore, considering that the component subjected to the highest von Mises stress is the piston rod, another mesh convergence analysis has been carried out for this case (Figure 29), the purpose of which is to obtain results that are independent of the mesh size, optimizing the balance between precision

and computational cost. Table 3 shows the element size values, von Mises stress (MPa), and relative error percentage for each iteration.

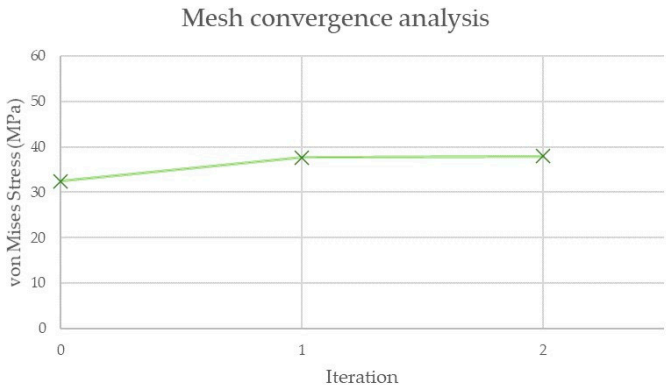

Figure 29. Maximum von Mises stresses obtained at each iteration.

Table 3. Results of mesh convergence analysis.

Element Size (mm)	Von Mises Stress (MPa)	Relative Error (%)	Iteration
5	32.46	Not Available	0
4	37.67	16.05	1
3.8	37.96	0.77	2

Thus, the element size applied to the piston rod was 3.8 mm, as the relative error with the previous iteration was 0.77% (less than 10%), thereby ensuring the accuracy of the simulation. Figure 30 shows the von Mises stress distribution of the ensemble, and Figure 31 shows the location of its maximum value (37.96 MPa), situated at the lower part of the piston rod at the junction with the crosshead, which is the same area obtained in the analysis of critical position 1.

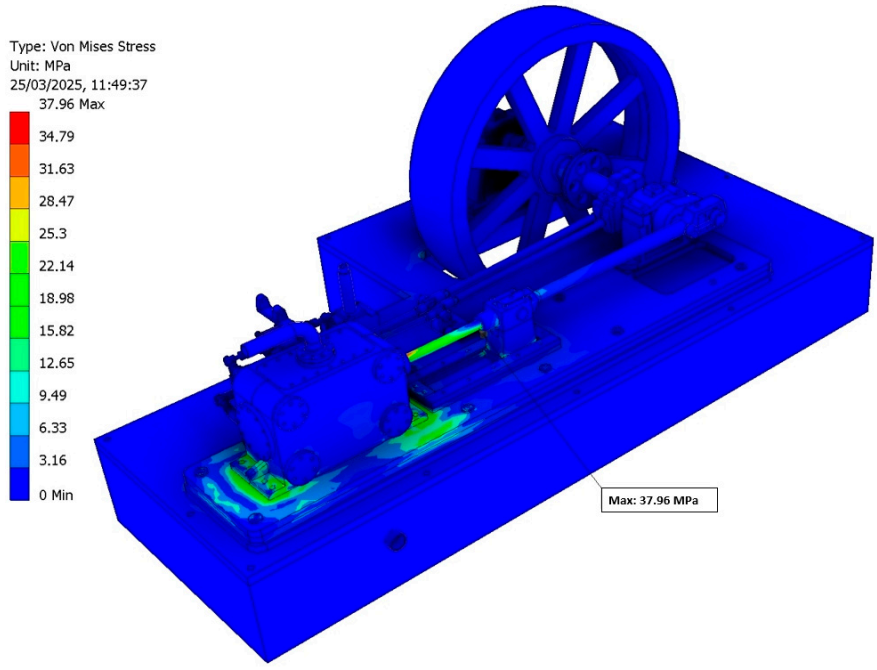

Figure 30. Distribution of von Mises stresses for a working pressure of 4.1 MPa.

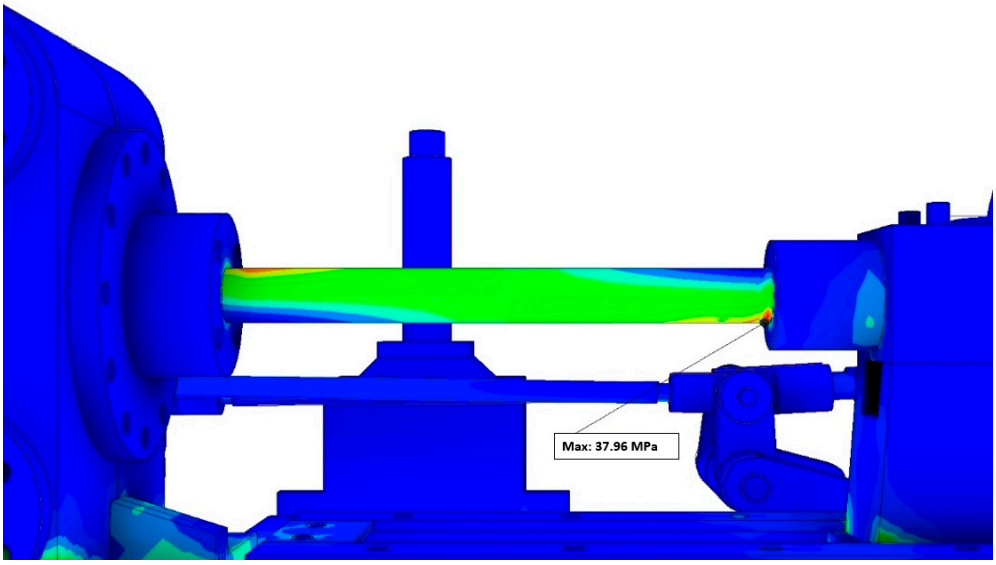

Figure 31. Location of the maximum value of the von Mises stress for a working pressure of 4.1 MPa.

The displacement distribution (Figure 32) was also obtained, shown with a scale factor ($\times$0.5) for improved visualization. Furthermore, analyzing the maximum obtained value of 0.05111 mm, located in the inlet steam pipe at the top of the cylinder block, it can be considered negligible as it is significantly smaller than the dimensions of the historical invention, considering its operation.

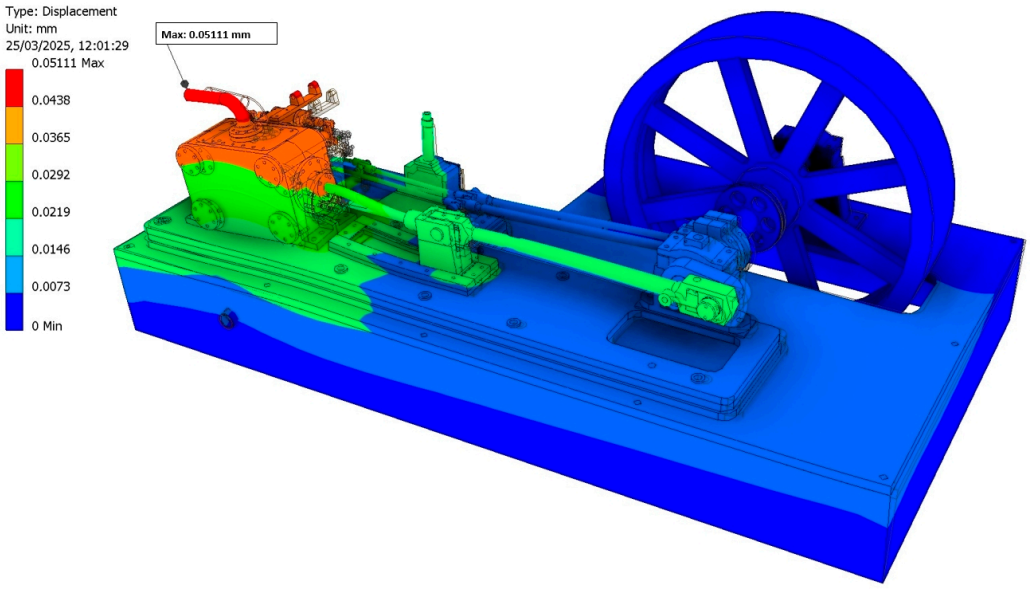

Figure 32. Distribution of displacements and location of the maximum value with a scale factor of $\times$0.5 for a working pressure of 4.1 MPa.

Finally, the safety factor distribution (Figure 33) and the location of its minimum value (2.01) (Figure 34) were also obtained, precisely at the cylinder liner, which is within the optimal design range.

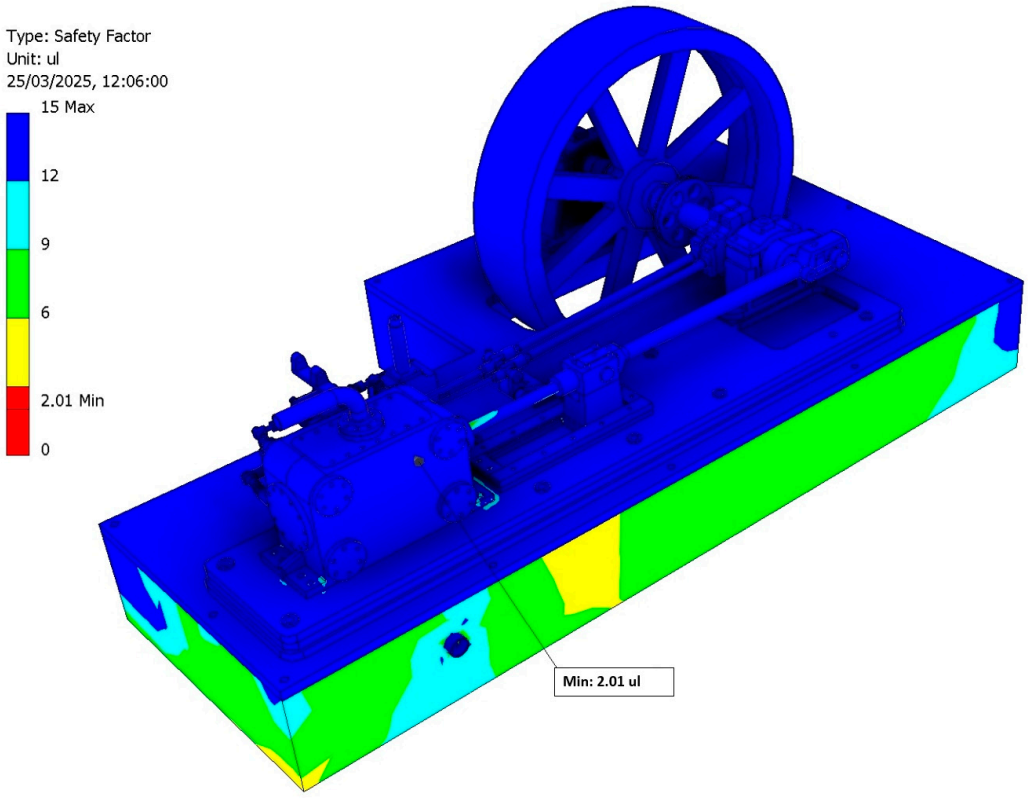

Figure 33. Distribution of the safety factor for a working pressure of 4.1 MPa.

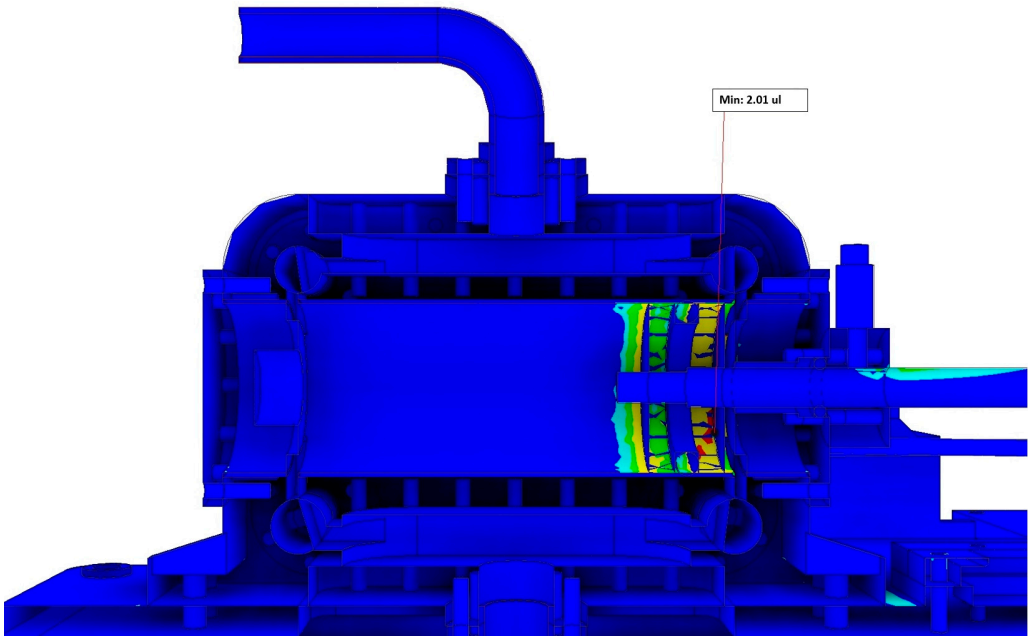

Figure 34. Location of the minimum value of the safety factor for a working pressure of 4.1 MPa.

4. Discussion

The results indicate that the maximum von Mises stress value is 49.14 MPa, located in the piston rod when it is at the top dead center (critical position 1). This result is significantly below the yield strength of the steel used in the rod (stainless steel). Furthermore, many components do not experience any load, suggesting that the steam engine design is clearly over-dimensioned. Additionally, the displacement results show that the piston rod undergoes buckling between the connection with the cylinder block and the crosshead.

This phenomenon could be the subject of future research to determine if this component meets the buckling failure criterion.

Regarding displacements, it is worth noting that the maximum values found in both critical positions are negligible, located at the top of the cylinder block. This is attributed to the steam inlet pipe being cantilevered. These results confirm the hypothesis of small deformations, allowing for calculations to be performed in the undeformed state using the Eulerian formulation method for discretization, thereby reducing computational cost. Moreover, the absence of significant deformations ensures minimal friction due to the relative movement between components.

From the perspective of optimizing the historical invention, to avoid over-dimensioning of the components, the proposed solutions include reducing thicknesses, optimizing the cross-sectional area, and considering lighter materials. This could lead to the more critical components of the invention, such as the piston, crosshead, connecting rod, or crankshaft, which endure the highest stresses, having a more compact configuration and potentially being cheaper to manufacture.

Similarly, to significantly reduce the maximum displacements caused by the cantilever, the lengths of the segments could be shortened, positioning the conduit closer to the cylinder block and decreasing the horizontal span. However, given that these displacements are negligible, it implies that the operation of the steam engine under the analyzed operating conditions is stable.

Furthermore, the safety factor is greater than unity, with a minimum value within the optimal design range for the maximum working pressure of 7.8 MPa (critical position 1). Therefore, this value can be used to determine the operating pressure of other geometrically similar machines through the technique of dimensional analysis. Likewise, with this maximum working pressure, observing the bottom dead center (critical position 2), which is the most restrictive condition for this magnitude, a safety factor greater than 2 is achieved in both critical positions.

Similarly, the minimum pressure value with which a safety factor of less than 4 (specifically 3.98) was verified to establish the working pressure range. This minimum pressure value is 4.1 MPa, obtained by observing the top dead center (critical position 1), which was the most restrictive condition (Figure 35).

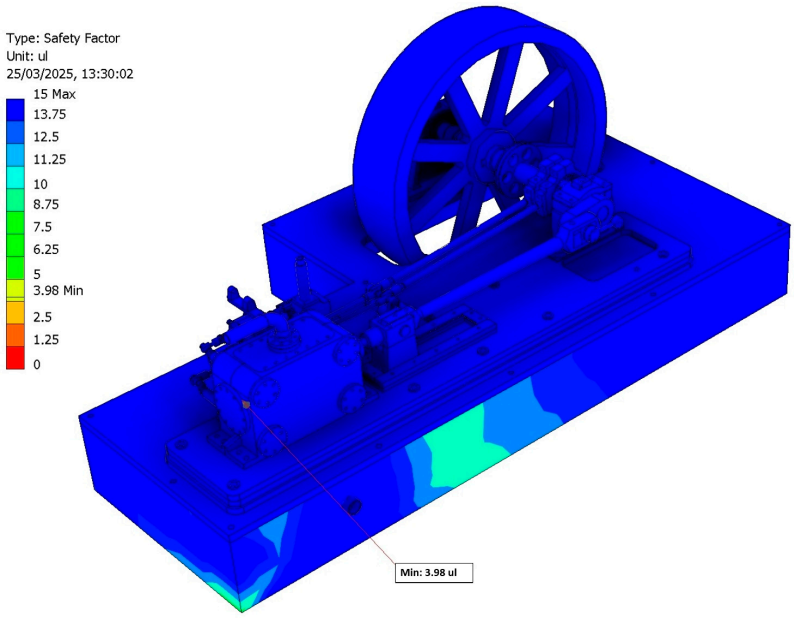

Figure 35. Distribution of the safety factor for a working pressure of 4.1 MPa at the top dead center (critical position 1).

Furthermore, it was verified that the safety factor was less than 4 (3.83) at the bottom dead center (Figure 36).

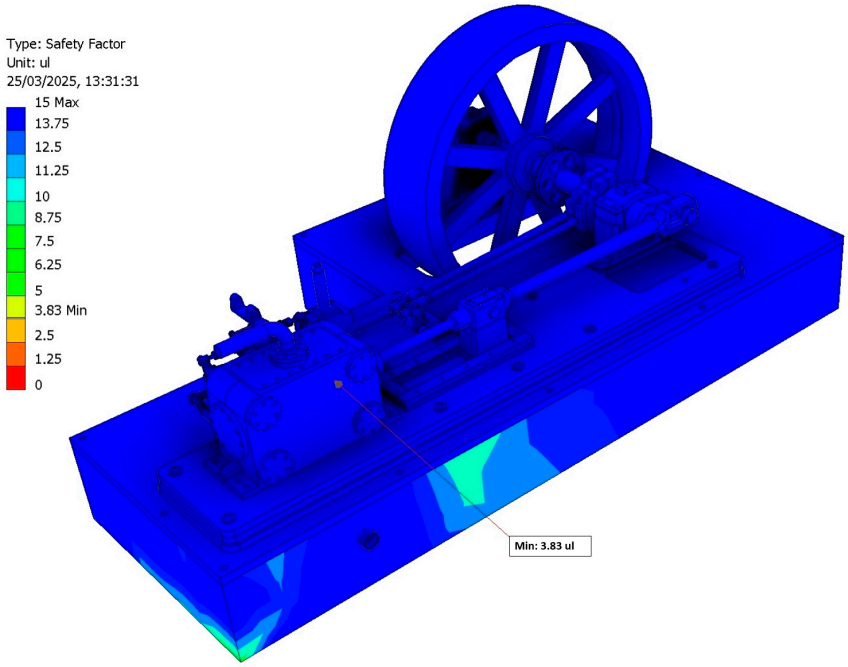

Figure 36. Distribution of the safety factor for a working pressure of 4.1 MPa at the bottom dead center (critical position 2).

Therefore, it can be concluded that the optimal range of working pressures for the steam at the admission for the historical invention analyzed, according to the design criterion of a safety factor between 2 and 4, corresponds to values ranging from 4.1 MPa to 7.8 MPa.

5. Conclusions

In this investigation, the design integrity of a historical invention by Arnold Throp, specifically a single-cylinder high-pressure steam engine with a Corliss valve gear, has been studied from a mechanical engineering perspective using FEM. Given the absence of a physical prototype of this invention available for laboratory testing, a reliable 3D CAD model was obtained. Consequently, this 3D CAD model was subjected to a linear static analysis utilizing the stress analysis module integrated within Autodesk Inventor Professional 2024 software, examining two critical positions: top dead center (critical position 1) and bottom dead center (critical position 2).

As any information regarding the operational conditions of the invention is entirely unknown, the primary objective of this research was to determine the optimal range of gauge pressures at the steam admission point of the engine (working pressures) to ensure a safety factor between 2 and 4, in accordance with current optimal design criteria. This approach aims to achieve design efficiency.

Following mesh refinement, a mesh convergence analysis was conducted through an iterative process, yielding a relative error of 3.11% (below the 10% threshold established to conclude the iterative process) with an average element size of 3.8 mm in the third iteration for critical position 1, and a relative error of 0.77% with an average element size of 3.8 mm in the third iteration for critical position 2. The simulation confirmed that the optimal range of working pressures should be between 4.1 and 7.8 MPa.

Thus, for a working pressure of 7.8 MPa, a maximum von Mises stress of 49.14 MPa was obtained for critical position 1 and 37.96 MPa for critical position 2, both located at the

lower part of the piston rod, specifically at the junction with the crosshead. Furthermore, regarding the safety factors, values of 2.09 for critical position 1 and 2.01 for critical position 2 were obtained, ensuring values within the optimal design range.

As future work, studies are proposed to avoid over-dimensioning of the steam engine by reducing thicknesses, optimizing the cross-sectional area, and considering lighter materials.

Author Contributions: Conceptualization, J.I.R.-S.; methodology, J.I.R.-S. and S.S.-G.; investigation, J.I.R.-S. and S.S.-G.; formal analysis, J.I.R.-S. and S.S.-G.; visualization, J.I.R.-S. and S.S.-G.; supervision, J.I.R.-S.; writing—original draft preparation, J.I.R.-S. and S.S.-G.; writing—review and editing, J.I.R.-S. and S.S.-G. All authors have read and agreed to the published version of the manuscript.

Funding: The research presented in this paper has been possible thanks to a collaboration grant from the Department of Engineering Graphics, Design and Projects of the University of Jaen obtained in the 2024 call from the Ministry of Education and Vocational Training of the Government of Spain.

Institutional Review Board Statement: Not applicable.

Informed Consent Statement: Not applicable.

Data Availability Statement: The original contributions presented in the study are included in the article. Further inquiries can be directed to the corresponding author.

Acknowledgments: We would like to thank the anonymous reviewers of this paper for their constructive suggestions and comments.

Conflicts of Interest: The authors declare no conflicts of interest.

References

1. Inkster, I. (Ed.) *History of Technology*; Bloomsbury Academic: London, UK, 2004; Volume 25.
2. Jenkins, R. *Links in the History of Engineering and Technology from Tudor Times*; The Newcomen Society at the Cambridge University Press: Cambridge, UK, 1971.
3. Thoendel, E. Simulation model of the thermodynamic cycle of a three-cylinder double-acting steam engine. *Chem. Prod. Process Model.* **2008**, *3*, 21. [CrossRef]
4. Yatsuzuka, S.; Niiyama, Y.; Fukuda, K.; Muramatsu, K.; Shikazono, N. Experimental and numerical evaluation of liquid-piston steam engine. *Energy* **2015**, *87*, 1–9. [CrossRef]
5. Wang, Y.; Zhou, Z.J.; Zhou, J.H.; Liu, J.Z.; Wang, Z.H.; Cen, K.F. Micro Newcomen steam engine using two-phase working fluid. *Energy* **2011**, *36*, 917–921. [CrossRef]
6. Ceccarelli, M.; Cocconcelli, M. Plans for a Course on the History of Mechanisms and Machine Science. In *Trends in Educational Activity in the Field of Mechanism and Machine Theory*; Springer: Cham, Switzerland, 2022; pp. 135–144. [CrossRef]
7. Cocconcelli, M.; Ceccarelli, M. Italian Teaching with Models from Mechanism Catalogues in 19th Century. In *Explorations in the History and Heritage of Machines and Mechanisms*; Springer: Cham, Switzerland, 2024; pp. 18–30. [CrossRef]
8. Ceccarelli, M.; Cocconcelli, M. Italian historical developments of teaching and museum valorization of mechanism models. *Machines* **2022**, *10*, 628. [CrossRef]
9. Throp, A. A model condensing Corliss engine: Part 1. *Model Eng.* **1982**, *149*, 223–224.
10. Throp, A. A model condensing Corliss engine: Part 2. *Model Eng.* **1982**, *149*, 328–331.
11. De Waal, J. Arnold Throp's Corliss Condensing Engine. 2018. Available online: https://modelengineeringwebsite.com/Corliss_drawings.html (accessed on 19 March 2025).
12. Rojas-Sola, J.I.; Sánchez-García, S. Study of the Engineering Design of a Single-Cylinder High-Pressure Steam Engine with a Corliss Valve Gear. *Appl. Sci.* **2025**, *15*, 3587. [CrossRef]
13. Cerdà Pérez, M. *Arqueología industrial: Teoría y Práctica*; Publicacions de la Universitat de València: Valencia, Spain, 2008. (In Spanish)
14. Inglis, W. On the Corliss expansion valve-gear for stationary engines. *Proceeding Inst. Mech. Eng.* **1992**, *19*, 177–194. [CrossRef]
15. Li, J. The Corliss Steam Engine and the United States Economy in the Late Nineteenth-Century. Master's Thesis, University of Delaware, Delaware, DE, USA, 2007.
16. Rosenberg, N.; Trajtenberg, M. A General-Purpose Technology at work: The Corliss steam engine in the late-nineteenth-century United States. *J. Econ. Hist.* **2004**, *64*, 61–99. [CrossRef]

17. Ferguson, E.S. Power and influence—The Corliss steam engine in the centennial era. *Ann. N. Y. Acad. Sci.* **1984**, *424*, 225–246. [CrossRef]
18. Goodheart, A. The machine of the Myth + The Corliss-engine in machinery-hall at the centennial-exposition in Philadelphia 1876. *Des. Q.* **1992**, *155*, 24–28. [CrossRef]
19. Abrams, B.A.; Li, J.; Mulligan, J.G. Did Corliss Steam Engines Fuel Urban Growth in the Late Nineteenth Century? Less Sanguine Results. *J. Econ. Hist.* **2008**, *68*, 1172–1176. [CrossRef]
20. Liu, Y.; Huang, M.; An, Q.; Bai, L.; Shang, D.Y. Dynamic characteristic analysis and structural optimization design of the large mining headrame. *Machines* **2022**, *10*, 510. [CrossRef]
21. Rojas-Sola, J.I.; Barranco-Molina, J.C. Study of the mechanical behavior of a single-cylinder horizontal steam engine with a crosshead trunk guide through the finite-element method. *Appl. Sci.* **2024**, *14*, 5878. [CrossRef]
22. Rojas-Sola, J.I.; Barranco-Molina, J.C. Technical feasibility of a two-cylinder entablature steam engine with a parallel motion crosshead: An analysis from mechanical engineering. *Appl. Sci.* **2024**, *14*, 6597. [CrossRef]
23. Shih, R.H.; Jumper, L. *Parametric Modeling with Autodesk Inventor 2024*; SDC Publications: Mission, KS, USA, 2023.
24. Zienkiewicz, O.C.; Taylor, R.L.; Zhu, J.Z. *The Finite Element Method: Its Basis and Fundamentals*, 7th ed.; Butterworth-Heinemann: Oxford, UK, 2013.
25. Reddy, J.N. *An Introduction to the Finite Element Method*, 3rd ed.; McGraw-Hill: New York, NY, USA, 2006.
26. Logan, D.L. *A First Course in Finite Element Method*, 6th ed.; Cengage Learning: Stamford, CT, USA, 2016.
27. Oñate Ibáñez de Navarra, E. *Structural Analysis with the Finite Element Method. Linear Statics*, 1st ed.; Springer: Dordrecht, The Netherlands, 2013.
28. Hughes, T.J.R. *The Finite Element Method: Linear Static and Dynamic Finite Element Analysis*; Dover Publications, Inc.: New York, NY, USA, 2012.
29. Gere, J.M.; Goodno, B.J. *Mechanics of Materials*, 8th ed.; Cengage Learning: Stamford, CT, USA, 2012.